EXPERIMENTAL PULSED LASER, REMOTE CROSSWIND MEASUREMENT SYSTEM - FEASIBILITY STUDY AND DESIGN

J. Fred Holmes, et al

Oregon Graduate Center

Prepared for:

Army Electronics Command

July 1974

Unclassified

SECURITY CLASSIFICATION OF THIS PAGE (When Data Entered)

REPORT DOCUMENTATION PAGE		READ INSTRUCTIONS BEFORE COMPLETING FORM
1. REPORT NUMBER ECOM74-0094-1	2. GOVT ACCESSION NO.	3. RECIPIENT'S CATALOG NUMBER AD 786 647
4. TITLE (and Subtitle) PULSED LASER, REMOTE CROSSWIND MEASUREMENT SYSTEM Feasibility Study and Design		5. TYPE OF REPORT & PERIOD COVERED FINAL; 7 December 1973 - 30 June 1974 6. PERFORMING ORG. REPORT NUMBER
7. AUTHOR(s) J. Fred Holmes and J. Richard Kerr		8. CONTRACT OR GRANT NUMBER(s) DAAD07-74-C-0094
9. PERFORMING ORGANIZATION NAME AND ADDRESS The Oregon Graduate Center Department of Applied Physics & Electronic Science		10. PROGRAM ELEMENT, PROJECT, TASK AREA & WORK UNIT NUMBERS
11. CONTROLLING OFFICE NAME AND ADDRESS U.S. Army Electronics Command, Atmospheric Sciences Laboratory, White Sands Missile Range, New Mexico		12. REPORT DATE July 1974 13. NUMBER OF PAGES 42
14. MONITORING AGENCY NAME & ADDRESS(if different from Controlling Office)		15. SECURITY CLASS. (of this report) Unclassified 15a. DECLASSIFICATION/DOWNGRADING SCHEDULE

16. DISTRIBUTION STATEMENT (of this Report)

Approved for public release; distribution unlimited.

17. DISTRIBUTION STATEMENT (of the abstract entered in Block 20, if different from Report)

18 SUPPLEMENTARY NOTES

Details of illustrations in this document may be better studied on microfiche

19 KEY WORDS (Continue on reverse side if necessary and identify by block number)

Remote Crosswind Measurement, Laser Anemometer, Atmospheric Turbulence

20. ABSTRACT (Continue on reverse side if necessary and identify by block number)

The feasibility determination and design for an experimental, pulsed laser, diffuse target, remote crosswind measurement system is described. The system consists of a laser transmitter, a diffuse target and a receiver.

A unique scheme utilizing a double-pulsed, Q-switched ruby laser is used to measure the slope of the time delayed autocovariance function at zero time delay which under appropriate conditions is proportional to the weighted

DD FORM 1 JAN 73 1473 EDITION OF 1 NOV 65 IS OBSOLETE

Unclassified

SECURITY CLASSIFICATION OF THIS PAGE (When Data Entered)

20. Abstract (continued)

average crosswind along the laser propagation path. The receiver consists of two silicon vidicons, a spinning disk for directing alternate pulses to the vidicons and appropriate scanning circuitry for generating a 10 x 10 array of apertures on each vidicon. Due to the pulsed nature of the system, spatial (ensemble) averages in lieu of time averages are utilized. The system can measure the autocovariance function and the slope of the time delayed autocovariance function at zero time delay for nine aperture spacings in two orthogonal directions and has the potential for two-dimensional, path resolved crosswind measurement.

Experimental Pulsed Laser, Remote Crosswind

Measurement System -- Feasibility Study and Design

Dr. J. Fred Holmes
Dr. J. Richard Kerr

Contractor: Oregon Graduate Center for Study and Research

Sponsor: U. S. Army Electronics Command, Atmospheric Sciences Laboratory, White Sands Missile Range, New Mexico 88002

Contract Number: DAA D07-74-C-0094

Effective Date of Contract: 7 December 1973

Contract Expiration Date: 30 June 1974

Amount of Contract: $65,000

Principal Investigator: Dr. J. Richard Kerr

Co-Investigator: Dr. J. Fred Holmes

Project Monitor: Mr. Thomas H. Pries

CONTENTS

INTRODUCTION

The feasibility of remotely determining the transverse wind velocity with a point-to-point, cw laser system is well established.[1,2,3] In recent work,[4,5] investigators have considered the extension of the technique to the use of a cw laser as well as ambient light, with a passive, diffuse target. In either case, the technique basically consists of relating the scintillation pattern on the receiver, to the frozen-in, transverse motion of the turbulence structure along the propagation path. The most successful cw method that has been used involves the measurement of the slope of the log amplitude covariance function at zero time delay.[1]

The field application for the wind measuring technique requires nearly instantaneous measurements. Although short time averages (e.g. 1-10 seconds) have been shown to produce satisfactory results in the cw approach, the use of a non-cooperative, diffuse target suggests the utilization of a pulsed laser source for useable signal levels at reasonable ranges.

In order to employ a pulsed laser and still make a temporal measurement as required for wind velocity, a double-pulse technique is used whereby two Q-switched laser pulses are generated at a time interval on the order of a millisecond. This interval appears to be appropriate for the employment of the covariance "slope at zero time lag" technique[1] and is compatible with current double-pulse laser technology.

Since the pulse technique precludes time averaging of the statistical quantities measured, spatial averaging is employed. Therefore the equivalent of an array of detectors had to be utilized in order to generate a sufficient number of samples of the instantaneous scintillation pattern to use spatial averaging. To the extent that the statistics of this pattern are invariant with lateral translation at the receiver (a safe assumption with the use of a diffuse target as a secondary source), such spatial averaging will give the desired

INTRODUCTION

The feasibility of remotely determining the transverse wind velocity with a point-to-point, cw laser system is well established.[1,2,3] In recent work,[4,5] investigators have considered the extension of the technique to the use of a cw laser as well as ambient light, with a passive, diffuse target. In either case, the technique basically consists of relating the scintillation pattern on the receiver, to the frozen-in, transverse motion of the turbulence structure along the propagation path. The most successful cw method that has been used involves the measurement of the slope of the log amplitude covariance function at zero time delay.[1]

The field application for the wind measuring technique requires nearly instantaneous measurements. Although short time averages (e.g. 1-10 seconds) have been shown to produce satisfactory results in the cw approach, the use of a non-cooperative, diffuse target suggests the utilization of a pulsed laser source for useable signal levels at reasonable ranges.

In order to employ a pulsed laser and still make a temporal measurement as required for wind velocity, a double-pulse technique is used whereby two Q-switched laser pulses are generated at a time interval on the order of a millisecond. This interval appears to be appropriate for the employment of the covariance "slope at zero time lag" technique[1] and is compatible with current double-pulse laser technology.

Since the pulse technique precludes time averaging of the statistical quantities measured, spatial averaging is employed. Therefore the equivalent of an array of detectors had to be utilized in order to generate a sufficient number of samples of the instantaneous scintillation pattern to use spatial averaging. To the extent that the statistics of this pattern are invariant with lateral translation at the receiver (a safe assumption with the use of a diffuse target as a secondary source), such spatial averaging will give the desired

result and the pulsed technique is fundamentally similar to the cw, time-averaging approach. However, the partial coherence of the laser and the characteristics of scintillations involving a diffuse source introduce new factors. These issues are pertinent for both the cw and pulsed systems and have been given some consideration by other investigators.[4,5]

The primary emphasis during Phase I of this investigation was on feasibility determination and design of an experimental, pulsed-laser, remote-crosswind measurement system utilizing the "slope" method. Accomplishments during the report period include:

Established a receiver concept for real time measurement of the average wind utilizing a pulsed source and diffuse target;

Established that use of a diffuse target with pulsed laser illumination for wind determination is feasible;

Designed and built an experimental transmitter and receiver system;

Established a test site and installed and tested the transmitter;

Developed a technique for processing the data to determine the wind; and

Established a conceptual design for a field system requiring realistic laser energy levels.

BACKGROUND

In non-saturated turbulence, the time delayed covariance function for the intensity is given by[4,6,7,8]

$$C_X(\rho,\tau) = 4\pi^2\, 0.033k^2 \int_0^L C_n^2(z)\, W_1(\rho,\tau,z)\, dz \qquad (1)$$

where

$$W_1(\rho,\tau,z) = \int_0^k u^{-8/3}\, J_o\left(u\left(\frac{\rho z}{L} - v(z)\tau\right)\right)$$

$$\cdot\, \mathrm{Sin}^2\left[\frac{u^2 z\,(L-z)}{2kL}\right] K_s^2\, K_r^2 \qquad du \qquad (2)$$

$$K_S = \frac{2J_1\left[\frac{u(L-z)\,Ds}{2L}\right]}{\frac{u(L-z)\,Ds}{2L}} \qquad (3)$$

and

$$K_R = \frac{2J_1\left(\frac{uzD_R}{2L}\right)}{\frac{uzD_R}{2L}} \qquad (4)$$

The parameters used in equations (1) - (4) are defined by

K_R^2 = Receiver Filter function

K_S^2 = Source Filter function

D_R = Receiver aperture diameter

D_S = Incoherent source diameter

L = Total propagation path length

z = Distance from source

$C_n^2(z)$ = Turbulence strength

$V(z)$ = Wind velocity

ρ = Receiver aperture separation

τ = Time delay

k = Wave number

A Kolmogorov spectrum has been assumed.

The slope with respect to τ of the time delayed covariance function can be found from (1) and is given by

$$M_X(\rho) = -\left.\frac{\partial C_X(\rho,\tau)}{\partial \tau}\right|_{\tau = o} \tag{5}$$

$$M_X(\rho) = (0.033)\, 4\pi^2 k^2 \int_o^L v(z) Cn^2(z) W_2(z,\rho)\, dz \tag{6}$$

where

$$W_2(z,\rho) = \int_o^k u^{-5/3} J_1(u\rho)\, \mathrm{Sin}^2\left(\frac{u^2 z}{2k}\right) K_s^2\, K_R^2\, du$$

Equations (1) and (6) hold for the log-amplitude. However, it is the intensity that is measured. This can be accounted for by normalizing (1) and (6) by the variance since it has been shown[6,8] that the normalized covariance of the log-amplitude, amplitude and intensity are equal for the non-saturated case. The normalized expressions are then given by

$$C_{IN}(\rho',\tau) = \frac{C_I(\rho',\tau)}{C_I(o,o)} = \frac{\int_o^1 C_n^2(W) F_1(W,\rho',\tau)\, dw}{\int_o^1 C_n^2(W) F_3(W)\, dw} \tag{7}$$

$$M_{IN}(\rho') = \frac{M_I(\rho')}{C_I(o,o)} = \frac{\beta^{-1}\int_o^1 C_n^2(W) V(W) F_2(W,\rho')\, dw}{\int_o^1 C_n^2(W) F_3(W)\, dw} \tag{8}$$

where

$$F_1(W,\rho',\tau) = \int_o^{k\beta} q^{-8/3} J_o\left[q\left(\rho' W - \frac{V(W)\tau}{\beta}\right)\right] \cdot \mathrm{Sin}^2\left[\frac{q^2 W(1-W)}{4\pi}\right] K_s'^2 K_R'^2\, dq \tag{9}$$

$$F_2(W,\rho') = \int_o^{k\beta} q^{-5/3} J_1(q\rho' W)\, \mathrm{Sin}^2\left[\frac{q^2 W(1-W)}{4\pi}\right] K_s'^2 K_R'^2\, dq \tag{10}$$

$$F_3(W,\rho') = \int_o^{k\beta} q^{-8/3} \mathrm{Sin}^2\left[\frac{q^2 W}{4\pi}(1-W)\right] K_S'^2 K_R'^2\, dq$$

$$K_S' = 2J_1\left[\frac{q(1-W)\,D's}{2}\right] \Big/ \frac{q(1-W)\,D's}{2} \tag{11}$$

and

$$K_R' = 2J_1\left[\frac{qW\,D_R'}{2}\right] \Big/ \frac{qW\,D_R'}{2} \tag{12}$$

and where the following variable changes have been made

$$W = \frac{z}{L}$$

$$q = u\beta$$

$$\beta = \sqrt{\lambda L}$$

$$D_S' = \frac{D_S}{\sqrt{\lambda L}}$$

$$D_R' = \frac{DR}{\sqrt{\lambda L}}$$

$$\rho' = \frac{\rho}{\sqrt{\lambda L}}$$

Equations (7) and (8) represent the theoretical basis upon which remote probing of the turbulence and crosswind velocity is based. Equation (7) could be used to determine the average wind velocity by finding the time delay τ at which it has a peak value.[8,9] However, if the turbulence and/or wind is non-uniform, multiple peaks occur. Also, the scintillation pattern tends to evolve with time. Consequently this method is not very useful.

Equation (7) is linear in $C_n^2(z)$ and non-linear in $V(z)$. It could be used to determine the wind velocity along the path,[9] but the non-linear

relationship to V(z) makes it difficult. At zero time delay, equation (7) is independent of the velocity and depends linearly on $C_n^2(z)$. The "slope" function, Equation (8), is linearly dependent on the product of wind velocity V(z) and the turbulence $C_n^2(z)$. Equations (7), with zero time delay, and (8) can at least in principle be solved for the turbulence and wind profiles.[10-14]

If the turbulence is assumed to be uniform, then $C_n^2(z)$ can be taken out of the integrals in (8) and it becomes

$$M_{I_N}(\rho') = \beta^{-1} \frac{\int_0^1 V(W) F_2(W,\rho')\, dw}{\int_0^1 F_3(W)\, dw} \qquad (13)$$

The "slope" function in this case is proportional to a path weighted average of the velocity distribution along the propagation path and has been used quite successfully for cw remote wind sensing.[1,5] If the wind velocity is also constant along the path, then (13) becomes

$$M_{I_N}(\rho') = \beta^{-1} V \frac{\int_0^1 F_2(W,\rho')\, dw}{\int_0^1 F_3(W)\, dw} \qquad (14)$$

The slope function in this case is proportional to the crosswind velocity.

In a field situation, both the turbulence and the wind may be non-uniform along the propagation path. Consequently a field system may require the capability for path resolved wind measurements. There are several possible techniques that might be used to accomplish this. In principal it could be done by varying the path weighting function[4,15,16], i.e., if the weighting function takes on the form of a "delta" function, then the turbulence strength and wind

velocity would be determined at the point along the path that the weighting function was non-zero.

Another approach that looks very promising and has been used with some success [9-11] is to use the covariance function and the slope of the covariance to obtain the turbulence strength and wind speed as a function of position along the propagation path. Each of these functions is represented by an integral involving the wind speed and/or the turbulence strength. By measuring the covariance and "slope" at several detector spacings, the integral equations can be used to resolve $C_N(z)$ and $V(z)$ to some degree along the path. An important issue in any technique is the required accuracy on the measurements versus the accuracy of the path resolved parameter.[10,11,17,18] As the path resolution increases, the required accuracy of the measurements increases very rapidly. Consequently, a practical limit appears to be the utilization of measurements at three or four detector spacings.

EXPERIMENTAL PROTOTYPE DESIGN

As shown in the previous section, the covariance function and the slope of the time delayed covariance function at zero time delay contain information about the strength of turbulence and the crosswind velocity along the propagation path. Consequently, an instrument that can measure these two functions has the capability for remotely determining the turbulence strength and crosswind. This is the basis on which an experimental prototype was designed.

Work by other investigators has been restricted to cw sources where the propagation path is direct to the receiving system (double-ended system) or a cooperative target such as retro-reflector[19,20] is used (single-ended system), or passive (ambient) illumination is used. Under these conditions, an acceptable signal to noise ratio can be achieved at reasonable transmitter power levels. However, the proposed applications of the work sponsored under this project requires a single-ended system operating against a non-cooperative target which can be viewed as a perfectly diffuse surface with reflectivity of approximately 0.1. Under this constraint, a cw system would require excessive transmitter power levels. However, preliminary analysis indicates that a pulsed system operating at about the 1 Joule level could be designed with adequate signal to noise ratio (S/N).

The primary noise sources in the system are the Poisson fluctuations of detector current and thermal noise in the electronics. For a given pulse energy, as the pulse width decreases the instantaneous power increases. Consequently, the detector signal current increases and eventually its Poisson fluctuation becomes the dominant noise source. If the receiver is gated synchronously with the transmitted pulses, at this point it would be signal shot noise limited. Therefore, in a direct detection optical system, the signal to noise ratio for a given total energy increases as the pulse duration is made shorter.[21] There is of course a limit on how short the transmitted pulses or ultimately the receiver gate width can be made. In our

particular case, the minimum transmitted pulse width is around 10-30 nanoseconds. However, it will not be necessary to go to this limit in gating the receiver in order to meet the system requirements.

For a photodiode type detector working into an ideal (infinite bandwidth) operational amplifier operating in the current mode, the S/N is given[22] approximately by

$$\frac{S}{N} = \frac{R_f^2 I_s^2}{B\left[R_f^2 I_n^2 + 4KT F_n + \left(\frac{R_f}{R_i} + 1\right)^2 e_n^2 + \left(\frac{R_f}{rd}\right)^2 e_{bn}^2\right]} \qquad (15)$$

where

e_n = Amplifier voltage noise$/\sqrt{Hz}$

e_{bn} = bias voltage noise$/\sqrt{Hz}$

R_f = Feedback resistance

r_d = detector shunt resistance

B = bandwidth

$R_i = \frac{R_1 r_d}{R_1 + r_d}$

R_1 = Amplifier Input resistance

$I_n^2 = \frac{4KT}{r_d} + 2e\,(I_s + I_d + I_1)$

I_s = detector signal current

I_d = detector dark current

I_1 = amplifier input current

If I_n^2 is dominated by $2eI_s$ and $R_f^2 I_n^2$ dominates the other denominator terms in (15), then the system operation is signal shot noise limited and (15) becomes

$$\frac{S}{N} = \frac{I_s}{2eB} \tag{16}$$

If B is made equal to $1/\tau$ where τ is the pulse width (or Gate time), and using

$$I_s = \frac{U_R e \eta}{h\nu\tau}$$

where

U_R = Received energy

η = detector efficiency

equation (16) becomes

$$\frac{S}{N} = \frac{U_R \eta}{2h\nu} \tag{17}$$

where

$$U_R = U_T \frac{\text{(Target Reflectance)}}{\pi} \cdot \frac{\pi}{4} \cdot \left(\frac{\text{Receiver Diameter}}{\text{Range}}\right)^2 \tag{18}$$

For a target reflectance of 0.1, a receiver diameter of 2 cm a transmitted energy of 1 Joule and a range of 3 Km, signal shot noise limited operation yields an S/N of almost 60 db which should be adequate. It should be noted that (17) depends linearly on the transmitted energy. Consequently, if the transmitted energy is decreased by a factor of ten yielding 100 millijoules, the S/N decreases by only 10 db.

Figure 1 shows the effect of receiver gate time on the signal to noise ratio for the above described conditions and with the following electronics parameters used for illustration

τ = Gate Time

$B = 1/\tau$

$R_f = 10^6$ ohms

$r_d = 10^8$ ohms

$R_i = r_d$

$I_s = U_r/\tau$

$I_d = 5 \times 10^{-8}$

$I_l \rightarrow$ Negligible

$e_n = 30 \times 10^{-9}$ V·Hz$^{-1/2}$

$e_{b_n} = 30 \times 10^{-9}$ V·Hz$^{-1/2}$

From Figure 1 it appears that signal shot noise limited operation can be achieved with a gate time of around 10^{-6} seconds.

Several types of detectors were considered for the experimental prototype including silicon vidicons, arrays of photodiodes and charge coupled devices. The presently available charge coupled devices are several orders of magnitude inferior from a noise standpoint than the other devices and were rejected on that basis. The silicon vidicon (which is essentially a large array of photodiodes read out with an electron beam) and photodiodes have similar noise characteristics. However, for purposes of an experimental prototype, both have advantages and disadvantages. The silicon vidicon is limited in beam current and sweep speed which in turn limits the minimum gate time and prevents signal shot noise limited operation. However, it allows a very flexible and readily changeable design due to the need for only a single set of optics (vice an array) and the ability to electronically generate and control the receiving array. This is a considerable advantage and led us to choose the silicon vidicon for the first experimental prototype. It should be noted that at this point it appears a

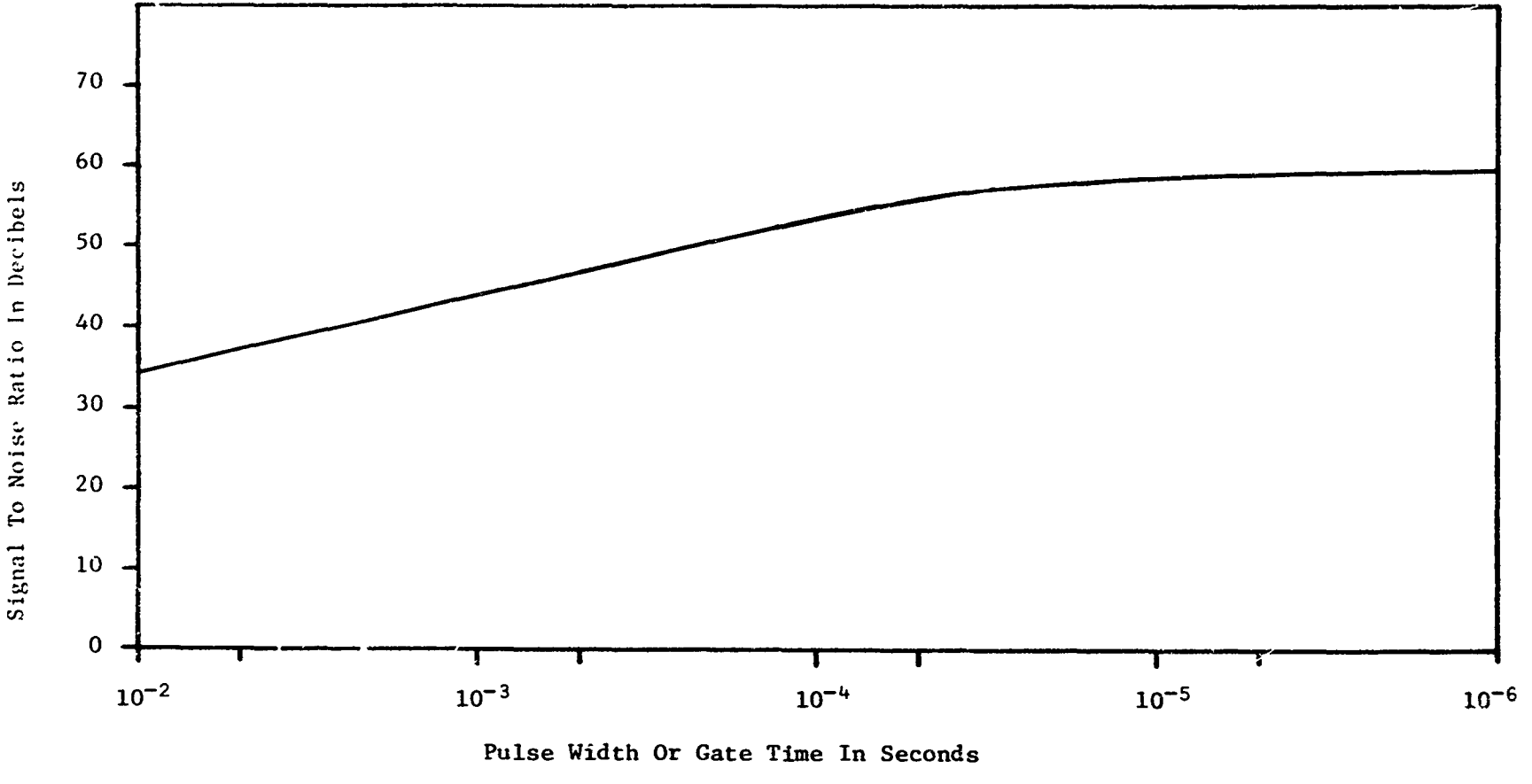

Figure 1. Signal to Noise Ratio Versus Gate Time.

photodiode array will be necessary for a field system due to the need for signal shot noise limited operation. To compensate for the slower gate time (smaller S/N) with the silicon vidicons, a special target material is being used. It is a high gain Scotchlite paper which represents a quasi-diffuse scatterer. When illuminated by a cw coherent source, the Scotchlite paper exhibits strong speckle, characteristic of a diffuse target. Use of this material allows the effect of a diffuse target material to be assessed at a much lower illumination level than would normally be required for the silicon vidicon system. The Scotchlite has a gain relative to that of a perfectly diffuse surface of around 40 π. The signal to noise ratio for the silicon vidicon system is estimated to be in excess of 70 db at 1.6 Km. The maximum background illumination that is expected to be encountered at the test site is 0.03 Watt/cm^2/Sr/μm. By limiting the field of view of the receiver to 3 milliradians and using a 10^{-2} μm bandpass filter in front of the vidicons, the received background power density is of the order of 3×10^{-10} Watts/cm^2. To further limit the background, a mechanical shutter (spinning disk) is used to mechanically gate the receiver for around 1 millisecond. The received background energy then is of the order of 3×10^{-13} Joules/cm^2 as compared to around 10^{-9} Joules/cm^2 at 1.6 Km for the received signal.

The purpose of the receiver is to provide intensity measurements from which the covariance function and the "slope" of the covariance function can be calculated. The latter function can be derived by calculating the covariance at two closely spaced points in time. This is accomplished by utilizing two transmitter pulses separated in time by 10^{-3} second.

Since the quantity being measured (received intensity) is a random variable, a single measurement would not yield a good estimate of the expected value. With a cw system, a time average can be used to statistically average the signal. It appears that good results are being obtained with temporal averaging times of 1 to 10 seconds.[1,4] Since the pulsed system samples only one instance in time, a spatial average must be used.

In order to obtain the required spatial averaging, the equivalent of an array of detectors is required. In addition, since the two pulses are only a millisecond apart, the array must be read out quickly or two arrays must be used in conjunction with a means for directing the return from the second pulse to the alternate array. We are using two silicon vidicons to realize the arrays. The face of each vidicon is divided electronically into a 10 x 10 matrix of equally spaced cells Each element in the matrix is scanned and a digital number generated that represents the integrated flux over the cell. The location of the center of each cell (i.e. the spacing) is fixed in the present arrangement but could be made electronically variable. However, the size of each cell is controlled electronically and gives us the capability to vary the effective aperture of each cell. A spinning disk and a hole and mirror arrangement are used to direct the two received pulses to one vidicon or the other (see Figure 2). The 2 x 100 numbers representing the two scintillation patterns are temporarily stored in a memory and then recorded by punching a paper tape for later processing. The measurement system is extremely flexible which will aid in assessing the effects of detector spacing and aperture size on system performance. It will allow a variety of techniques for converting the information in the scintillation patterns into wind speed to be evaluated and has the capability for determining two-dimensional path resolved wind. The receiver is illustrated schematically in Figure 2.

The receiver optical system consists of two lenses and a field of view limiting aperture. The scintillation pattern at the entrance aperture (first lens) is demagnified by a factor of approximately 14.3 and imaged onto a 1 cm diameter area on the vidicon face. For a 1.6 Km propagation path, this yields a cell spacing and cell aperture of 0.43 Fesnel zones ($\sqrt{\lambda L}$). The 10 x 10 array covers an area of 4.3 x 4.3 Fesnel zones. For the smallest cell spacing, this allows 90 spatial samples to be averaged. Of course all the samples are not completely independent. Data from individual cells can be

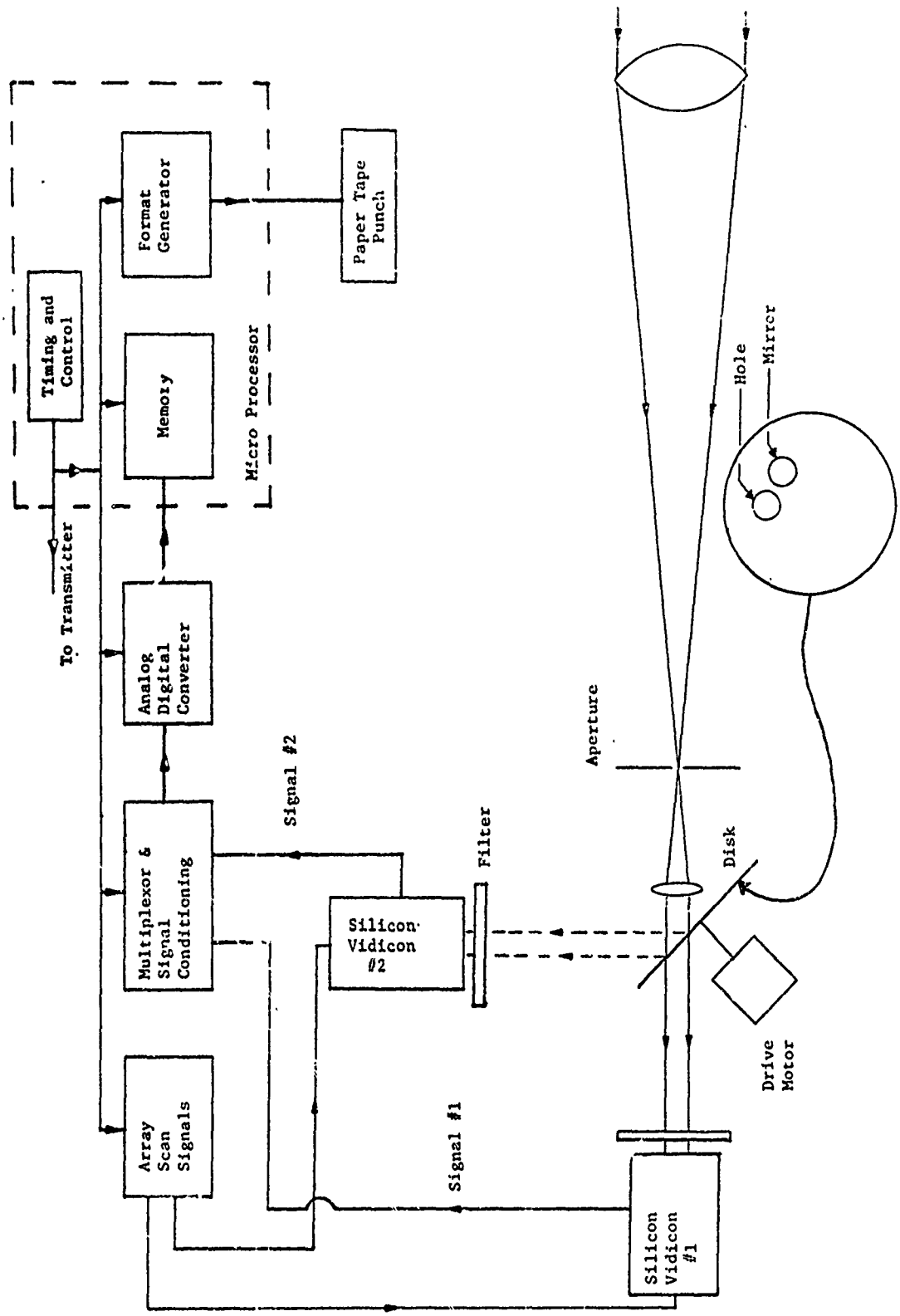

Figure 2. Receiver Diagram.

combined to form larger cells if desired and the second lens can be changed to decrease the spacing. The primary criterion on system performance is the error in estimating the crosswind. As the cell size increases more signal (average) is received, but the scintillation level decreases. Also, for a given cell spacing, as the cell size increases, the samples become more dependent which will increase the error. Because these effects are competing, there is probably an optimum cell size and spacing for a given number of cells and the optimum solution may also be a function of range and/or turbulence level. This will be studied during phase II.

The transmitter is shown schematically in Figure 3. The source is a double-pulse, Q-switched ruby laser. The requirement for the laser to produce two Q-switched pulses separated by about one millisecond was met by exciting the laser rod with a long pump pulse and Q-switching twice within the pump pulse interval. A double-pulse, Q-switched ruby laser meeting these requirements was available commercially (Apollo Lasers Inc.) for use in the system. The energy per pulse is approximately 0.5 Joule with a repetition rate of 6 pulse pairs per minute.

Ruby appears to be the best choice at the present time. However, in the future longer wavelengths may be seriously considered because of the reduced probability of saturation of scintillation at longer wavelengths. A small He-Ne laser is used for alignment and as a tracer beam for the ruby laser. This greatly facilitates steering the beam onto the target. It will not be required in a field system.

The 9.5 mm output beam of the ruby laser is beam expanded using a negative lens and a 320 mm mirror. This reduces the 3-5 milliradian divergence of the raw beam to around 10^{-4} radian which is the same order of magnitude as the maximum spread due to turbulence. A negative lens was required to avoid tightly focusing the raw beam, since it has enough energy to break down the air. The negative lens is on on a track that allows the beam to be focused to a spot at any

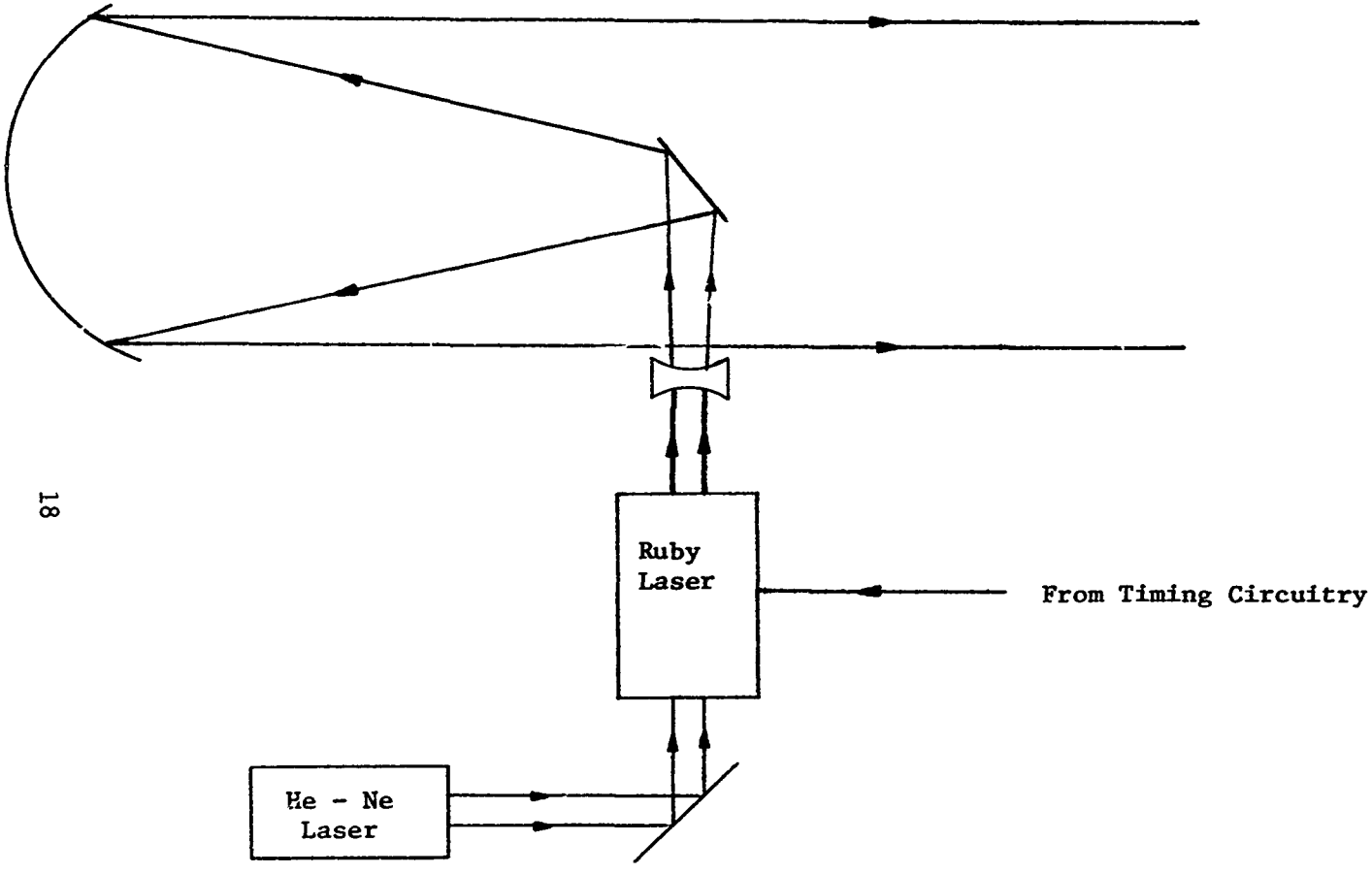

Figure 3. Transmitter Diagram

distance beyond a few hundred feet from the transmitter. The spot size in the absence of turbulence should be around 160 mm at 1.6 Km. As the turbulence increases, the spot size will increase. A larger spot size decreases the degree of scintillation and changes the covariance function. However, the larger spot size is caused by stronger turbulence which increases the measured effect. Consequently there are competing effects which tend to cancel each other. The change in the covariance function may also significantly affect the instrument calibration.

Another factor that must be considered is saturation. For a reasonably long, low path at visible or near-IR wavelengths, the scintillations will be "saturated" in moderate and strong turbulence.[6] This represents the multiple scattering realm, and affects the shape of the covariance curve and hence path-weighting.[4,23] For a system to cope with this phenomenon, it will probably be necessary that the degree of saturation be known or measured. Our measurement system can generate an estimate of the covariance function at 9 spatial separations. It may be possible that the degree of saturation can then be inferred from the covariance function. By using a model appropriate for the saturated condition[24] proper corrections can then be incorporated into the data processing. In this regard, the technique for determining the wind from the data may have to be self-adaptive. In addition, recent work by NOAA[25] indicates that the effects of saturation can be neutralized by appropriate choice of source and receiver aperture sizes. More study is needed in this area.

Photographs of the completed equipment are shown in Figures 4 - 6.

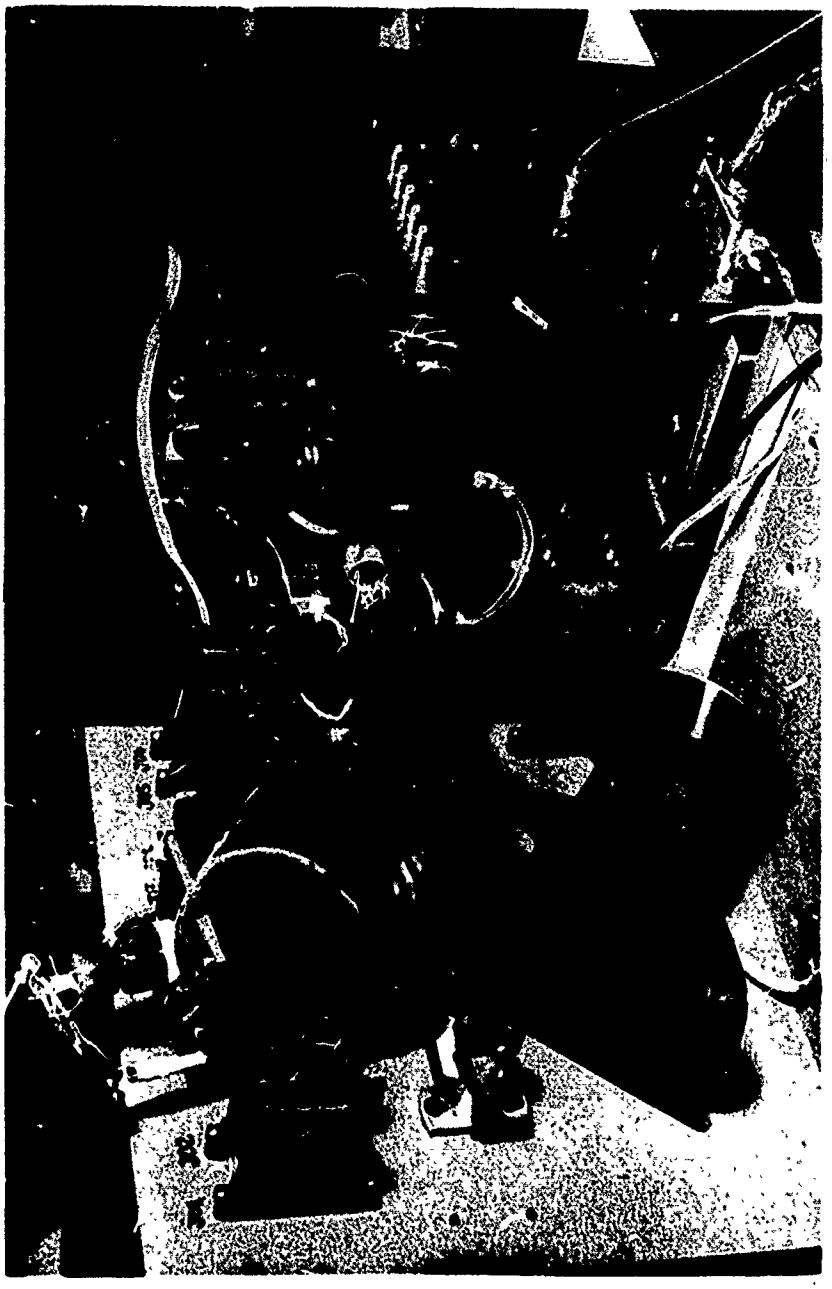

Figure 4. Receiver.

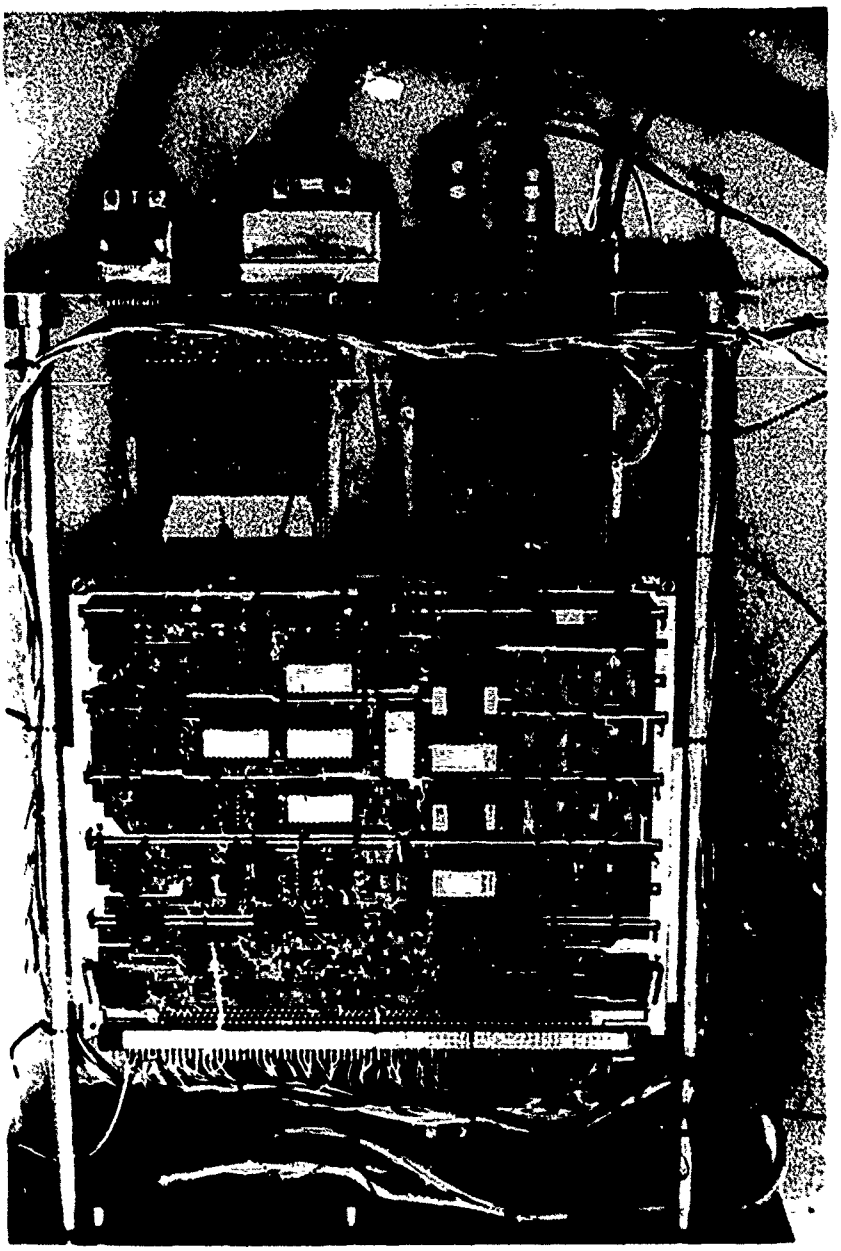

Figure 5. Microprocessor.

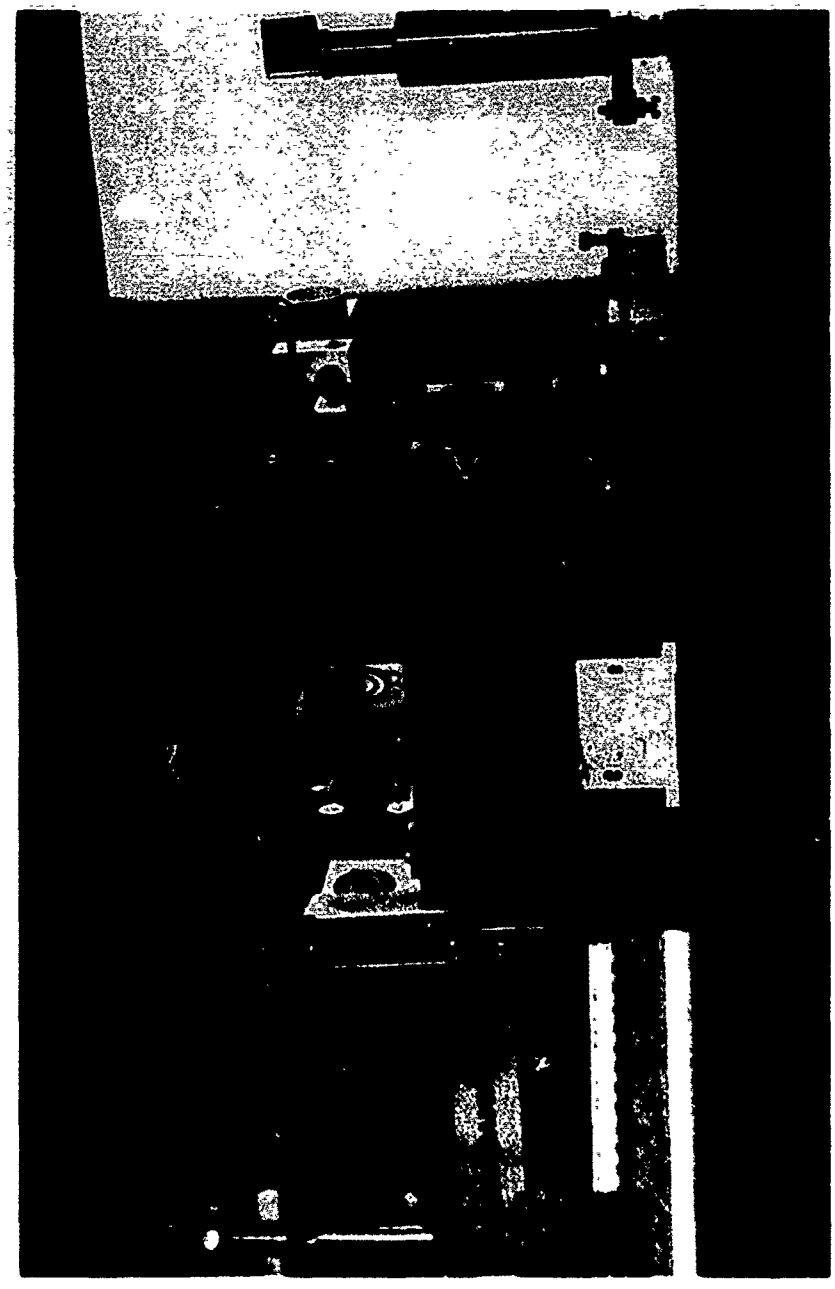

Figure 6. Transmitter Installation.

PROCESSING

The instrument described in the previous section records 200 numbers that are proportional to the total integrated intensity received by each cell in the array. From these data, the average intensity, variance and covariance function for each pulse and the slope of the covariance function at zero time delay are calculated.

The covariance of a random variable I(r,t) can be expressed as

$$C_I(r_2,t_2;r_1,t_1) = \langle [I(r_2,t_2) - \overline{I(r_2,t_2)}][I(r_1,t_1) - \overline{I(r_1,t_1)}] \rangle \quad (19)$$

If the process is wide sense stationary and locally homogeneous, then the covariance function only depends on the coordinate differences

$$\rho = |r_2 - r_1|$$

$$\tau = t_2 - t_1$$

and (19) becomes

$$C_I(\rho,\tau) = \langle [I(r_2,t_2) - \bar{I}][I(r_1,t_1) - \bar{I}] \rangle \quad (20)$$

The data is reduced on the basis of equation (20).

Since we are dealing with two, two-dimensional arrays of data, it is convenient to use three subscripts to identify the array location and pulse. For example consider I(J,K,N).

J = array row

K = array column

N = pulse number (1 or 2)

Using this notation and approximating the ensemble average by a finite spatial average, the average intensity, variance and normalized covariance function are then given by

$$\bar{I} = \frac{1}{100}\left[\sum_{J=1}^{10}\sum_{K=1}^{10} I(J,K,N)\right] \tag{21}$$

$$\sigma_I^2 = C_I(o,o) = \frac{1}{100}\left[\sum_{J=1}^{10}\sum_{K=1}^{10} [I(J,K,N) - \bar{I}]^2\right] \tag{22}$$

$$C_{I_N}(ns',o) = \frac{1}{10\,\sigma_I^2}\left[\sum_{J=1}^{10}\left[\frac{1}{(10-n)}\sum_{K=1}^{10-n} [I(J,K,N) - \bar{I}][I(J,K+n,N) - \bar{I}]\right]\right] \tag{23}$$

where S' is the normalized cell spacing, n takes on the integer values 1 through 9.

The slope of the covariance function at zero time delay can be expressed as

$$M_{I_N}(\rho') = \left.\frac{\partial C_{I_N}(\rho',\tau)}{\partial\tau}\right|_{\tau=o}$$

$$= \lim_{\tau_o \to o} \frac{C_{I_N}(\rho',\tau o) - C_{I_N}(\rho',-\tau o)}{2\tau o} \tag{24}$$

With $2\tau o$ chosen to be 10^{-3} seconds, the limit restriction can be removed without causing a significant error.[1] Doing this and rewriting the covariance functions in a form more readily identifiable with the arrays and pulses, (24) becomes

$$M_{I_N}(\rho') = \frac{C_{I_N}(X_2,t_2;X_1,t_1) - C_{I_N}(X_2,t_1;X_1,t_2)}{2\tau o} \tag{25}$$

Now using (19) this becomes,

$$M_{I_N}(\rho') = \frac{1}{2\tau o} \langle [I(X_2,t_2) - \bar{I}][I(X_1,t_1) - \bar{I}] - [I(X_2,t_1) - \bar{I}][I(X_1,t_2) - \bar{I}] \rangle / \sigma_I(N = 1)\sigma_I(N = 2) \tag{26}$$

Using the subscript notation and approximating the ensemble average by a spatial average, the normalized "slope" function becomes

$$M_{I_N}(ns') = \frac{10^3}{10\,(10-n)\,\sigma_I\,(N = 1)\,\sigma_I\,(N = 2)} \sum_{J=1}^{10} \sum_{K=1}^{10-n} \Big[[I(J,K+n,2) - \bar{I}(N = 2)] [I(J,K,1) - \bar{I}(N = 1)] - [I(J,K+n,1) - \bar{I}(N = 1)][I(J,K,2) - \bar{I}(N = 2)] \Big] \tag{27}$$

The data stored in each array is not the intensity but a number proportional to the intensity. In addition, the proportionality constant will be different for each array. However, because of the way in which the covariance and "slope" functions are normalized, the results for these quantities are independent of the proportionality constants and the energy in each laser pulse and no related calibration is necessary. However, this does not compensate for any sensitivity variation across the tube face. If absolute data on the average intensity and variance is desired, then the two proportionality constants will have to be either measured or calculated.

To obtain the average wind, the measured slope is used in conjunction with equation (14) to obtain

$$V = \beta M_{I_N}(ns') \left[\frac{\int_0^1 F_3(W)\, dw}{\int_0^1 F_2\left(W,\, ns'\right) dw} \right] \tag{28}$$

where $\beta = \sqrt{\lambda L}$

$M_{I_N}(ns')$ is the measured "slope" function and the quantity in brackets is a known function that can be calculated numerically with the aid of a computer. It has been calculated for the case

$$\rho' = \frac{ns}{\sqrt{\lambda L}} = 0.43$$

$$D'_R = 0.43$$

$$D'_S = 4.85$$

and

$$L = 1.6 \text{ Km}$$

For this case

$$V = 2.725 \times 10^{-2} M_{I_N} (0.43) \text{ m sec}^{-1} \qquad (29)$$

The proportionality constant is a function of the detector spacing and size, the source size and the path length. The detector spacing(s) and size are known and the path length will be known even in the field application, since a range finder will either be integrated into the system or coupled in externally. However, the source size will in general be a function of turbulence level and its effect on accuracy and calibration needs to be evaluated.

The instrument generated binary data tape begins with the following sequence of symbols which indicate the beginning of a data block: 1,0,# of bytes in data record (low byte first), 0,0. This is followed by the data block which consists of the 200 data words from the array plus 7 extra channels that can be used to record in situ measurements of wind speed, Cn^2 etc. for evaluation. A data word consists of two 6 bit bytes (12 binary digits) each of which has a parity (odd) check. The binary, 12 bit analog to digital conversion gives a resolution of one part in 4096 which should be down into the noise level.

The data is sequenced onto the tape alternately from array one and array two. For example, I(1,1,1) is punched followed by I(1,1,2), followed by I(1,2,1) etc. The array location is sequenced along each

row to the end and then shifts down to the next lower row without retracing. For example I(1,10,2) is followed by I(2,10,1).

The binary data on the instrument generated tape is converted using the Graduate Center PDP 11 computer to ASC II, and a new tape generated for use in processing the data. The data is processed using the program shown in Appendix A which also contains a sample of the computer generated output. The program prints out the data from the two arrays in the proper sequence and then calculates and prints out the average intensity, variance, covariance function and "slope" function. The data used in this example is hypothetical and is used merely to check out the program.

EXPERIMENTAL PROGRAM

Measurements will be made at an established field site over a 1.6 Km path with very uniform terrain. A small building complete with heat, light, power, communications and an optical table completely isolated from the building was constructed to house the experimental system. Figure 7 shows the field site facility.

Emphasis during preliminary phases of the experimental work will be centered around measuring the covariance function and average cross-wind velocity with the experimental system and comparing the results with the calculated covariance function and in situ wind measurements. As noted earlier, the covariance function changes with source size. In order to control this parameter, the target size will at first be restricted to a diameter of $4.85\sqrt{\lambda L}$ and the beam adjusted at very low turbulence levels to fill the entire target. The calculated covariance curve for this case is shown in Figure 8 and the corresponding wind weighting function is shown in Figure 9. It can be seen from Figure 10 that the weighting is peaked up toward the receiver.

During this phase of the work, the transmitter was operated at the field site and photographs were made of the received scintillation patterns from the double pulse ruby laser. Two cameras, an electronic shutter, a rotating disk with a hole and mirror, the receiver optics and electronics to synchronize firing of the laser with the disk were used. The rotating disk directed the scintillation pattern from the first laser pulse to one camera and the second pulse to the other camera. High speed infrared film (Kodak) was used to record the patterns with the Scotchlite target at 500 meters and 1.6 Km. Representative scintillation patterns are shown in Figures 10 - 12. Normal looking scintillation patterns were obtained at both ranges. The primary scale size appears to be appropriate for the path length and there appears to be no discernible speckle present. The length of the longest cross hair (from cross to edge of aperture) is approximately 8.5 inches. The patterns were recorded at night under very low turbulence conditions. The "rice grain" pattern in Figure 11 is

thought to be due to a very light rain. As can be seen from the photographs, the electronic synchronization with the disk was not perfect and consequently part of the patterns were occluded by the disk. This will not be a problem with the actual receiver in that a "real time" response will be available while adjusting the synchronization. The overall results from the photographs of the scintillation patterns tends to indicate that speckle will not be a problem.

Figure 7. Field Site Facility.

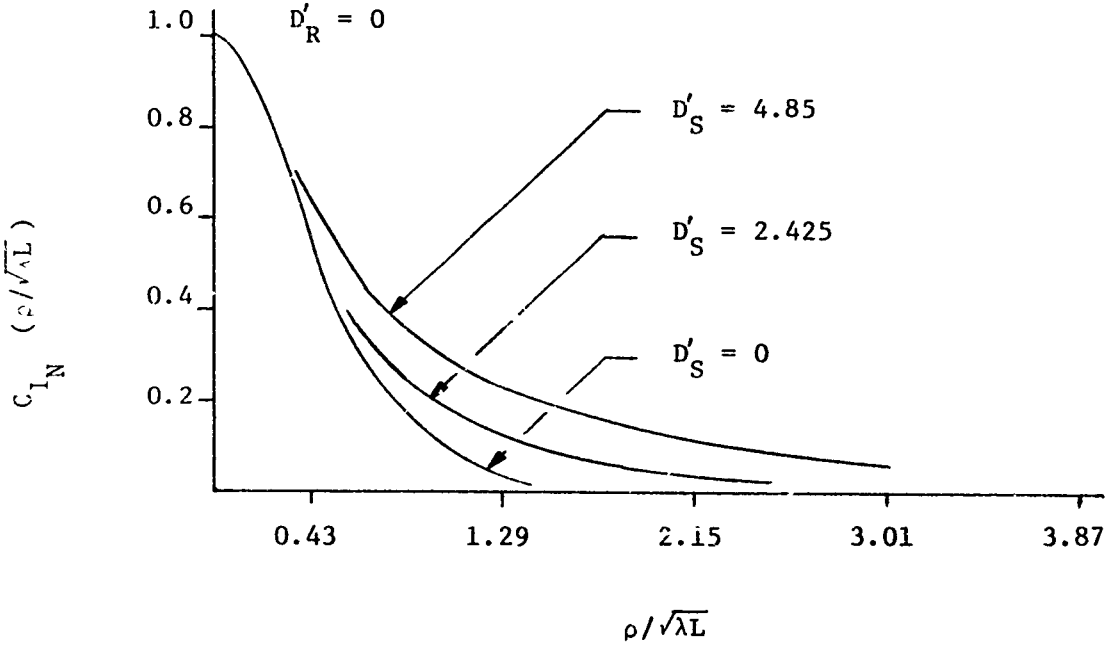

Figure 8. Calculated Covariance Curve.

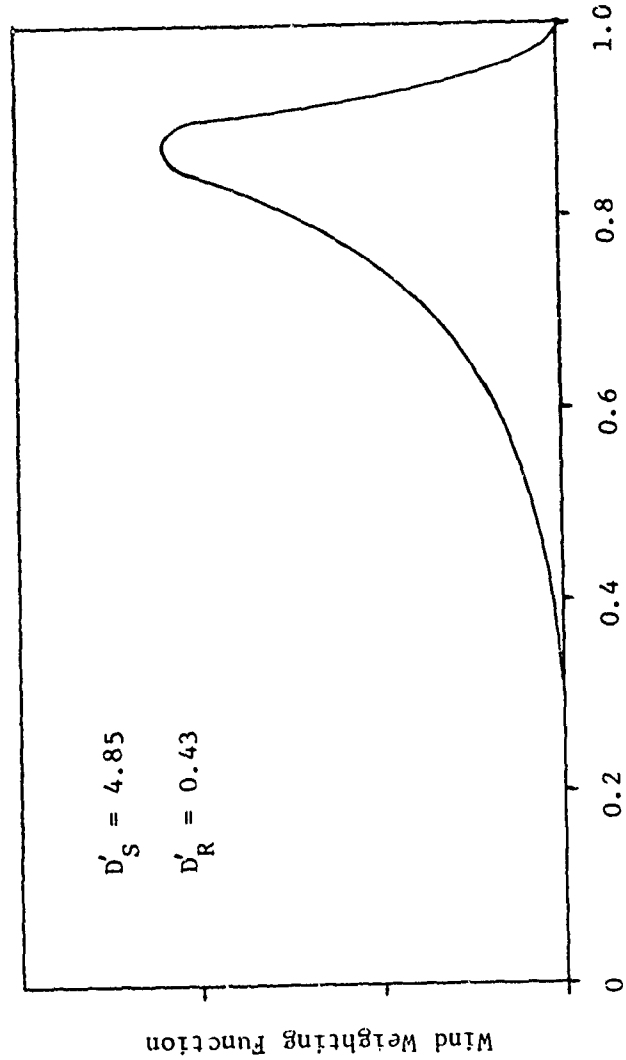

Figure 9. Calculated Wind Weighting Function.

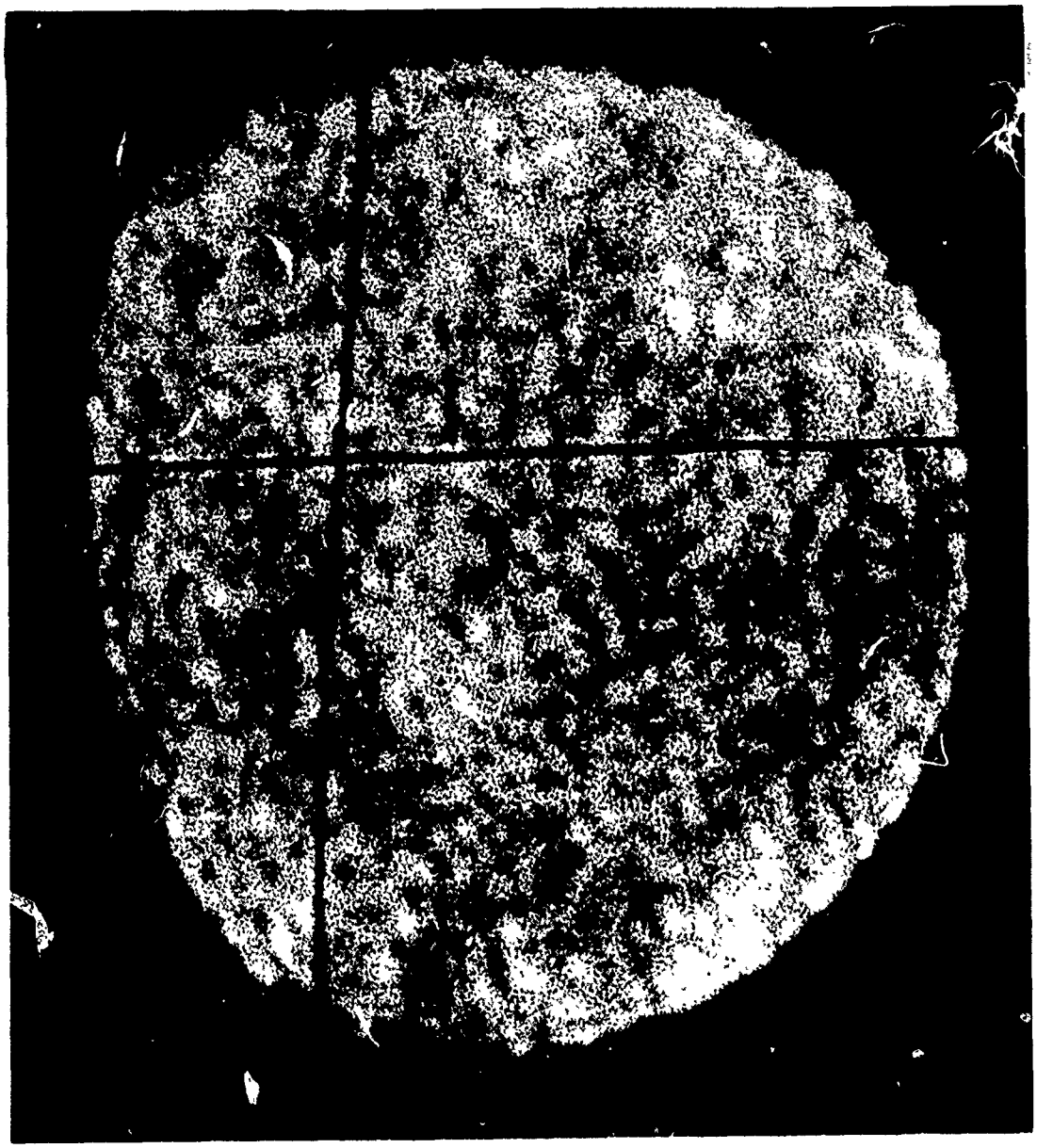

Figure 10. Scintillation Pattern, 500 Meters.

Figure 11. Scintillation Pattern, 500 Meters.

Figure 12. Scintillation Pattern, 1.6 Kilometers.

REFERENCES

1. Lawrence, R. S., G. R. Ochs, and S. F. Clifford, 1972, "The Use of Scintillations to Measure Average Wind Across a Light Beam," Appl. Opt., 11, 239.

2. Ochs, G. R., and G. F. Miller, 1972, "Pattern Velocity Computers - Two Types Developed for Wind Velocity Measurements by Optical Means," Rev. of Sci. Instrum., 43, 879.

3. Pries, T. H., and E. T. Young, 1974, "Evaluation of a Laser Crosswind System," United States Army Electronics Command Research and Development Technical Report, ECON-5546.

4. Ochs, G. R., S. F. Clifford, and T. I. Wang, 1973, "A Feasibility Study of an Optical Crosswind Monitor," NOAA Technical Memorandum WPL-10.

5. Ochs, G. R., and G. F. Miller, 1973, "The NOAA Optical Crosswind System," NOAA Technical Memorandum WPL-9.

6. Lawrence, R. S., and J. W. Strohbehn, 1970, "A Survey of Clear-Air Propagation Effects Relevant to Optical Communications," Proc. IEEE, 58, 1523.

7. Lutomirski, R. F., et al., 1973, "Degradation of Laser Systems by Atmospheric Turbulence," RAND Corporation Report R-1171-ARPA/RC.

8. Lee, R. W., and J. C. Harp, 1969, "Weak Scattering in Random Media, with Applications to Remote Probing," Proc. IEEE, 57, 375.

9. Fried, D. L., 1969, "Remote Probing of the Optical Strength of Atmospheric Turbulence and of Wind Velocity," Proc. IEEE, 57, 415.

10. Shen, L. C., 1970, "Remote Probing of Atmospheric and Wind Velocity by Millimeter Waves," IEEE Transactions on Antennas and Propagation, AP-18, 493.

11. Henegan, J. M., and A. Ishimaru, 1974, "Remote Determination of the Profiles of the Atmospheric Structure Constant and Wind Velocity Along a Line-of-Sight Path by a Statistical Inversion Procedure," IEEE Transactions, AP-22, 457.

12. Peskoff, A., 1971, "Theory of Remote Sensing of Wind Velocity Profiles," Proc. IEEE, 59, 324.

13. Peskoff, A., 1968, "Theory of Remote Sensing of Clear Air Turbulence Profiles," J. Opt. Soc. Am., 58, 1032.

14. Peskoff, A., 1968, "Inversion of the Correlation Function of a Spherical Wave Propagating Through the Atmosphere," TRW System Group Report 99900-6692-RO-00, Redondo Beach, California.

15. Wang, Ting-i, et al., 1974, "Wind and Refractive-Turbulence Sensing Using Crossed Laser Beams," NOAA Technical Memorandum.

16. Ochs, G. R., et al., 1974, "Development of a Ground-Based Optical Method for Measuring Atmospheric Turbulence Aloft," NOAA Technical Memorandum.

17. Twomey, S., and H. B. Howell, 1967, "Some Aspects of the Optical Estimation and Microstructure in Fog and Clouds," Appl. Opt., 6, 2125.

18. Twomey, S., 1974, "Information Content in Remote Sensing," Appl. Opt., 13, 942.

19. Smith, J., 1973, "Folded Path Weighting Function for a High Frequency Spherical Wave," J. Opt. Soc. Am., 63, 1095.

20. Smith, J., T. H. Pries, K. J. Skipka, and M. A. Hamiter, 1972, "High Frequency Plane-Wave Filter Function for a Folded Path," J. Opt. Soc. Am., 62, 1183.

21. Kerr, J. R., 1967, "Microwave-Bandwidth Optical Systems," Proc. IEEE, 55, 1686.

22. Hamstra, R. H., and P. Wendland, 1972, "Noise and Frequency Response of Silicon Photodiode Operational Amplifier Combination," Apl. Opt., 11, 1539.

23. Dunphy, J. R., and J. R. Kerr, 1973, "Scintillation Measurements for Large Integrated-Path Turbulence," J. Opt. Soc. Am., 63, 981.

24. Clifford, S. F., et al, 1974, "Saturation of Optical Scintillation by Strong Turbulence," J. Opt. Soc. Am., 64, 148.

25. Clifford, S. F., and G. R. Ochs, 1974, "The Effects of Saturation of Scintillation on Laser Wind Sensing," Presented at the Meeting on Optical Propagation Through the Atmosphere, University of Colorado, Boulder, Colorado.

APPENDIX A

```
005 DIM I1(10,10),I2(10,10),L1(10),L2(10),A(2),V(2)
006 DIM X1(10,10),X2(10,10),S1(10),M1(10),C1(2,9),M3(9)
010 OLD
015REM_READ IN CELL DATA AND CONVERT SEQUENCE
020 FOR J=0TO9
025 FOR K=0TO9
030 INPUT I1(J,K),I2(J,K)
035 NEXT K
040 NEXT J
045 FOR J=1TO9 STEP 2
050 FOR K=0TO9
055 LET M=9-K
060 LET L1(M)=I1(J,K)
065 LET L2(M)=I2(J,K)
070 NEXT K
075 FOR K=0TO9
080 LET I1(J,K)=L1(K)
085 LET I2(J,K)=L2(K)
086 NEXT K
090 NEXT J
095 REM_DATA NOW IN NORMAL MATRIX FORM
096 PRINT
100 PRINT "FIRST ARRAY"
101 FOR J=0TO9
110 FOR K=0TO9
115 PRINT I1(J,K),
120 NEXT K
125 NEXT J
130 PRINT "SECOND ARRAY"
135 FOR J=0TO9
140 FOR K=0TO9
145 PRINT I2(J,K),
150 NEXT K
155 NEXT J
156 PRINT
160 REM_CALCULATE AVERAGE INTENSITY EACH TUBE
165 LET S=0.
170 LET M=0.
175 FOR J=0TO9
180 FOR K=0TO9
185 LET S=S+I1(J,K)
190 LET M=M+I2(J,K)
195 NEXTK
200 NEXT J
205 LET A(1)=S/100
210 LET A(2)=M/100
```

```
215 REM CALCULATE VARIANCE
220 LET S=0.
225 LET M=0.
230 FOR J=0TO9
235 FORK=0TO9
240 LET S=S+I1(J,K)*I1(J,K)
245 LET M=M+I2(J,K)*I2(J,K)
250 NEXTK
255 NEXT J
260 LET V(1)=S/100.-A(1)*A(1)
265 LET V(2)=M/100.-A(2)*A(2)
270 PRINT "PULSE","AVERAGE INTENSITY","VARIANCE"
275 PRINT 1,A(1),,V(1)
280 PRINT 2,A(2),,V(2)
281 PRINT
285 REM CONVERT I DATA TO ZERO MEAN AND NORMALIZE BY VARIANCE
290 FOR J=0TO9
295 FOR K=0TO9
300 LET X1(J,K)=(I1(J,K)-A(1))/SQR(V(1))
305 LET X2(J,K)=(I2(J,K)-A(2))/SQR(V(2))
310 NEXT K
315 NEXT J
320 REM CALCULATE COVARIANCE FOR 9 SPACINGS
325 FOR S=0TO8
330 LET M=10-S-2
335 LET S2=0.
340 LET M2=0.
345 FOR J=0TO9
350 LET S1(J)=0.
355 LET M1(J)=0.
360 FORK=0TOM
365 LET S1(J)=S1(J)+X1(J,K)*X1(J,K+S+1)
370 LET M1(J)=M1(J)+X2(J,K)*X2(J,K+S+1)
375 NEXT K
376 LET S2=S2+S1(J)
380 LET M2=M2+M1(J)
385 NEXT J
390 LET C1(1,S)=S2/10./(M+1)
395 LET C1(2,S)=M2/10./(M+1)
400 NEXT S
410 PRINT "STEP","COVARIANCE PULSE ONE","COVARIANCE PULSE TWO"
415 FOR J=0TO8
420 PRINT J+1,C1(1,J),,C1(2,J)
425 NEXT J
426 PRINT
430 REM CALCULATE SLOPE
```

```
435 FOR S=0TO8
440 LET M=10.-S-2
445 LET S2=0.
450 FOR J=0TO9
455 LET S1(J)=0.
460 FORK=0TOM
465 LET S1(J)=S1(J)+X2(J,K+S+1)*X1(J,K)-X1(J,K+S+1)*X2(J,K)
470 NEXT K
475 LET S2=S2+S1(J)
480 NEXT J
485 LET M3(S)=1000.*S2/10./(M+1.)
490 NEXT S
495 PRINT "STEP","SLOPE OF COVARIANCE"
500 FOR J=0TO8
510 PRINT J+1,M3(J)
520 NEXT J
530 STOP
540 END
```

```
 FIRST ARRAY
  1             2             1             2             1
  2             1             2             1             2
  1             2             1             2             1
  2             1             2             1             2
  1             2             1             2             1
  2             1             2             1             2
  1             2             1             2             1
  2             1             2             1             2
  1             2             1             2             1
  2             1             2             1             2
  1             2             1             2             1
  2             1             2             1             2
  1             2             1             2             1
  2             1             2             1             2
  1             2             1             2             1
  2             1             2             1             2
```

SECOND ARRAY

2	1	2	1	2
1	2	1	2	1
2	1	2	1	2
1	2	1	2	1
2	1	2	1	2
1	2	1	2	1
2	1	2	1	2
1	2	1	2	1
2	1	2	1	2
1	2	1	2	1
2	1	2	1	2
1	2	1	2	1
2	1	2	1	2
1	2	1	2	1
2	1	2	1	2
1	2	1	2	1
2	1	2	1	2
1	2	1	2	1
2	1	2	1	2
1	2	1	2	1

PULSE	AVERAGE INTENSITY	VARIANCE
1	1.5	.25
2	1.5	.25

STEP	COVARIANCE PULSE ONE	COVARIANCE PULSE TWO
1	-1	-1
2	1	1
3	-1	-1
4	1	1
5	-1	-1
6	1	1
7	-1	-1
8	1	1
9	-1	-1

STEP	SLOPE OF COVARIANCE
1	0
2	0
3	0
4	0
5	0
6	0
7	0
8	0
9	0

```
STOP AT LINE  530
READY
READY
SAVE
```